

# Formation of hierarchical structures from functionalized multi-walled carbon nanotubes in aerosil containing solutions

Alexander P. Kuzmenko<sup>1</sup>, Thet Phyto Naing<sup>1</sup>, Andrey E. Kuzko<sup>1</sup>, Alexey V. Kochura<sup>1</sup>, Myo Min Than<sup>1</sup>, Nay Win Aung<sup>1</sup>

<sup>1</sup> Southwest State University, 94 50 let Oktyabrya Str., Kursk 305040, Russia

Corresponding author: Alexander P. Kuzmenko (apk3527@mail.ru)

Received 24 September 2019 ♦ Accepted 6 December 2019 ♦ Published 30 March 2020

**Citation:** Kuzmenko AP, Naing TP, Kuzko AE, Kochura AV, Than MM, Aung NW (2020) Formation of hierarchical structures from functionalized multi-walled carbon nanotubes in aerosil containing solutions 6(1): 17–23. <https://doi.org/10.3897/j.moem.6.1.54811>

## Abstract

Specific features and regularities of self-assembly and self-organization of multi-walled carbon nanotubes (MWCNT) have been studied for diffusion-limited conditions (method of drops) in water-based (deionized water) colloidal solutions with aerosil exposed to DC electric fields with magnitudes of 15 to 25 V. Studies of hierarchical structure formation during drop evaporation in uniform electric fields have revealed the formation of 40–120 nm sized linear piecewise formations, 25–45 nm sized fractal structures and 250 nm sized diffuse structures from MWCNT – COOH + aerosil + H<sub>2</sub>O<sub>dw</sub>. The structures have been studied using confocal microscopy, X-ray diffraction, Raman scattering, atomic force microscopy, IR spectroscopy and scanning electron microscopy. The sizes of the observed micro- and nanostructures decrease following the hyperbolic law  $d = 1/U$  in the approximation  $d \rightarrow 2R$ , their growth rate increasing as  $U^2$ . We show that intense ultrasonication of functionalized MWCNT – COOH + aerosil + H<sub>2</sub>O<sub>dw</sub> in colloidal solutions causes the formation of the so-called “breathing” modes in axis centered single-walled carbon nanotubes. This is confirmed by short-wave Raman scattering excitation and enables the existence of both combined  $sp^2$ -hybridization types with  $\pi$ - and  $\sigma$ - carbon bonds and the metallic and semiconductor conductivity types in the material thus showing good promise of these structures for nanoelectronics.

## Keywords

self-organization and self-assembly, stabilized multiwalled carbon nanotubes,  $sp^2$ -hybridization,  $\pi$ - and  $\sigma$ -carbon bonds, controlled ordering of carbon nanotubes

## 1. Introduction

New methods of synthesizing carbon nanotubes (CNT), both single-walled (SWCNT) and multi-walled (MWCNT) ones, have been developed in recent years. CNT exhibit unique physicochemical properties:

- mechanical strength of up to 45 GPa;

- heat conductivity of up to 6000 W/(m × K);
- current density of up to 11 GA/cm<sup>2</sup> with a very low field emission voltage of 1–3 V/μm;
- high chemical and mechanical stability.

The properties of CNT are largely determined by their extremely high aspect ratio  $l/d = 10^6$  [1, 2]. These properties as well as the large number and high availability of CNT synthesis methods and approaches in the form of

SWCNT or MWCNT favor their high demand in the most rapidly developing branches of engineering [3]. For example, CNT can be used in nanoelectronics as cold field emitters whose operation is based on the Fowler–Nordheim field emission mechanism. Introduction of 15% MWCNT into a polystyrene matrix provides for a current density of 100 mA/cm<sup>2</sup> at a voltage of 2.2 V/μm [4]. These SWCNT and MWCNT are widely used in nanoelectronic devices, e.g. single-electron and field transistors, logic elements and memory cells [5]. Of special importance for this process is adhesion which increases twofold in vertical CNT on substrates, to 1.43 GPa in an electric field [6]. Nanoguides synthesized on these unidimensional carbon structures have natural advantages, e.g. absence of ohmic loss and optimum sizes for nanoelectronics. A physical restriction preventing a wider use of SWCNT and MWCNT is the minimum free energy principle which causes their uncontrolled structuring in the form of ropes, coils, globes etc. [7, 8]. The problems of uncontrolled aggregation [9] are cleared off by introducing SWCNT and MWCNT into polymer or metallic matrices [9] or CNT functionalization with carboxyl groups –COOH [10]. This method allows achieving self-assembly and self-organization by increasing the stability of CNT colloidal solutions [11–13].

Below we present data on the effect of electric fields on the self-organization of MWCNT – COOH + aerosil + H<sub>2</sub>O<sub>dw</sub> at different concentrations in colloidal solutions in deionized water (DW) with aerosil.

## 2. Experimental

The test specimens were CCVD-synthesized (Catalytic Chemical Vapor Deposition) MWCNT by Nanocyl, Nelguim with CoO based nanocatalysts. Inset of Fig. 1 shows a scanning electron microscopic (SEM) image (JEOL JSM LV6610, 3 nm spatial resolution) of the test MWCNT. The minimum diameter of these MWCNT is within 20 nm. The MWCNT had high purity (up to 90%) and the aspect ratio  $l/d = 10^3$ . MWCNT functionalization included the following steps: agitation for 5 h in an ultrasonic bath in an acid medium (H<sub>2</sub>SO<sub>4</sub> : HNO<sub>3</sub> = 3 : 1) at 42 °C. After cooling the solution was diluted with deionized water in an equilibrium ratio, filtered, washed and dried [12, 13].

The MWCNT functionalization degree in the initial and the as-treated conditions was determined using Fourier IR spectroscopy (Fig. 1) on a Nicolet iS50 IR spectrometer (Thermo Fisher Scientific, USA) at a spectral resolution of up to 0.125 cm<sup>-1</sup>. Functionalization increased the intensity of all the bands in the 624 to 3435 cm<sup>-1</sup> range by an order of magnitude. The valence oscillation band at 3435 cm<sup>-1</sup> shifted by 4 cm<sup>-1</sup> (O–H, –OH), the 1618 cm<sup>-1</sup> one shifted by 37 cm<sup>-1</sup>, the 1585 cm<sup>-1</sup> one shifted by 25 cm<sup>-1</sup> (the –C=C– and –C–C aromatic rings, respectively) and the 1036 cm<sup>-1</sup> one shifted by 8 cm<sup>-1</sup> (stretching vibrational C–O). The oscillation bands at 2920, 2850, 1128 and 624 cm<sup>-1</sup> disappeared but new ones emerged: at 1385 cm<sup>-1</sup> (symmetrical oscillations in COO<sup>-</sup>) and 1217 cm<sup>-1</sup> (stretch-

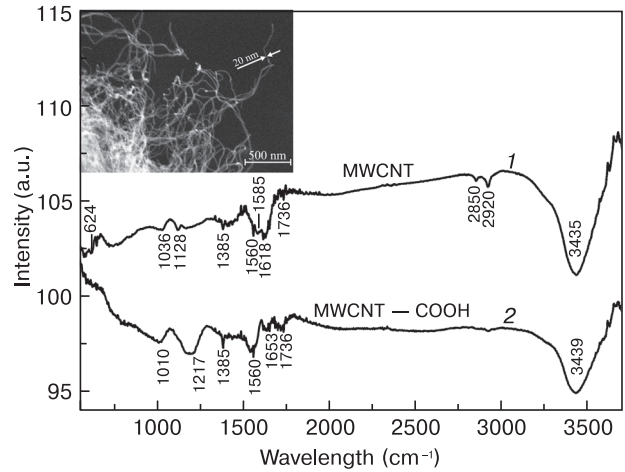


**Figure 1.** Fourier IR spectra of (1) initial and (2) functionalized MWCNT. Inset: SEM image of initial MWCNT (20 nm diameter).

ing vibrational oscillations of C–O). These changes in the Fourier IR spectra indicate MWCNT functionalization [1] and the formation of MWCNT–COOH complexes which increase the stability of the MWCNT colloidal solution by several times in comparison with earlier data [10].

Raman spectra were taken on an Omega Scope™ Raman microspectrometer (wavelength 532 nm, spectral resolution 0.8 cm<sup>-1</sup>). The Raman spectra contained the bands  $D = 1336\div 1353$  cm<sup>-1</sup> and  $G = 1567\div 1600$  cm<sup>-1</sup> the intensities of which were typical of MWCNT ( $I_D > I_G$ ). The intensity  $I_D$  of the band  $D$  for MWCNT–COOH increased in comparison with its initial value for MWCNT whereas the intensity  $I_G$  of the band  $G$  did not change. After functionalization the defectiveness of the structures expressed as  $I_D/I_G$  was  $\sim 1.4$  as compared with  $\sim 1.2$  for the initial MWCNT.

The MWCNT–COOH complexes were exposed to sequential ultrasonic agitation and dispersion in order to obtain a colloidal solution containing MWCNT – COOH + aerosil + H<sub>2</sub>O<sub>dw</sub>. The agitation and dispersion operations were carried out on a Volna UZTA-0,4/22-OM ultrasonic device (22 kHz ultrasonic oscillation frequency, max. 20 W power, up to 55 min exposure time with intervals after 5 min of continuous exposure). The colloidal solution prepared using this method was stable during the experiment and remains stable until now (after almost 2 years) compared with several months stability periods for typical solutions. The colloidal solution was applied using the drop method into an electrode gap (100, 500, 1000 and 1500 μm) of a circuit board produced by photolithography on a sital substrate capped with magnetron-sputtered copper, chromium or gold films (Fig. 2a) [10–12]. The electrodes were DC biased (15 to 25 V). The micrographs (Fig. 2b, c) show the cathode and the anode marked as + and –, respectively, with a 1500 μm gap between them.

The micro- and macroscopic reconstruction occurring in an electric field during evaporation of the colloidal solution drop was studied using confocal microscopy with a 0.46 digital aperture, an AIST-NT atomic force

microscope integrated into an OmegaScope Raman microscope and SEM. The particle dynamics was studied by video recording (frame rate 30 Hz, resolution  $704 \times 576$  px). The particles moved in the colloidal solution from the negative electrode to the positive one by analogy with earlier data [11–14].

### 3. Results and discussion

The structures forming in an electric field were systematized into fractal structures (FS), diffuse structures (DS) and piecewise linear structures (PLS). Their typical images are presented in Fig. 2*b, c*. One cannot clearly identify the boundary conditions for the formation of different structure types. SEM data indicate simultaneous growth of FS and PLS from the colloidal solution at the voltage  $U = 19$  V (Fig. 2*d–f*). However at  $U = 19.5$  V (Fig. 2*e, f*) not only PLS but also DS and PLS grew from the same solution (Fig. 2*b, c*). Figure 2*b* shows a confocal microscopic image of a dendritic FS growing from the colloidal solution at  $U = 19$  V (Fig. 2*d*). Analysis of Fig. 2*d* showed that the minimum diameter of discrete structures forming PLS grown from the colloidal solution was approx.  $D = 30$  nm. Assuming that the PLS were formed by discrete MWCNT – COOH with the minimum MWCNT diameter  $d = 20$  nm (Fig. 1, inset) we obtain that the total number of MWCNT in the PLS thickness could be  $S/s \sim D^2/d^2 \sim 12$  (here  $S$  and  $s$  are the areas of the cluster and the nanoparticle, respectively), i.e., an PLS is a “typical rope” in accordance with the terms put forward earlier [7].

The variety of structural formations growing from MWCNT – COOH is illustrated in Fig. 3. AFM images of PLS fragments grown from the colloidal solution at  $U = 19$  V (Fig. 3*a*) and at  $U = 19.5$  V (Fig. 3*d*) show that these PLS were formed by 40–120 nm sized MWCNT – COOH fragments (Fig. 3*d*), had significantly bent portions and consisted of discrete agglomerates only. The diameter of each of these agglomerates was the same, ranging from 25 to 45 nm (Fig. 3*e*, inset). These agglomerations were attributed to PLSs up to 450 nm in length, i.e., having the same length as those of most of the PLSs according to the SEM image (Fig. 2*d*). Note that MWCNT – COOH PLSs were observed earlier in a colloidal solution of sulfuric and nitric acids without an electric field; their diameter reached  $d = 550$  nm and the length was several times greater than  $d$  and reached several microns [12, 13]. Along with PLS fields AFM revealed the formation of spherical clusters with diameters of about 220 nm (Fig. 3*b, f*) consisting of discrete MWCNT – COOH. These structures can be systematized as “coils” of weaved carbon nanotubes [7].

The reconstruction of the chemical structure in the FS, DS and PLS described herein was traced from changes in the Raman spectrum for colloidal solution residue using Raman microscope spectroscopy with a spatial resolution of 500 nm. The formation of a specific structure under equilibrium conditions between carbon atoms with  $sp^2$ -hybridization is accompanied by growth of either  $\pi$ -bound elongated carbon clusters (sized up to several decades of microns) or  $\sigma$ -bound graphite structures as demonstrated in earlier works [11–13]. The formation of the bands  $D = 1336 \div 1353$   $\text{cm}^{-1}$  (A-type symmetry “defect

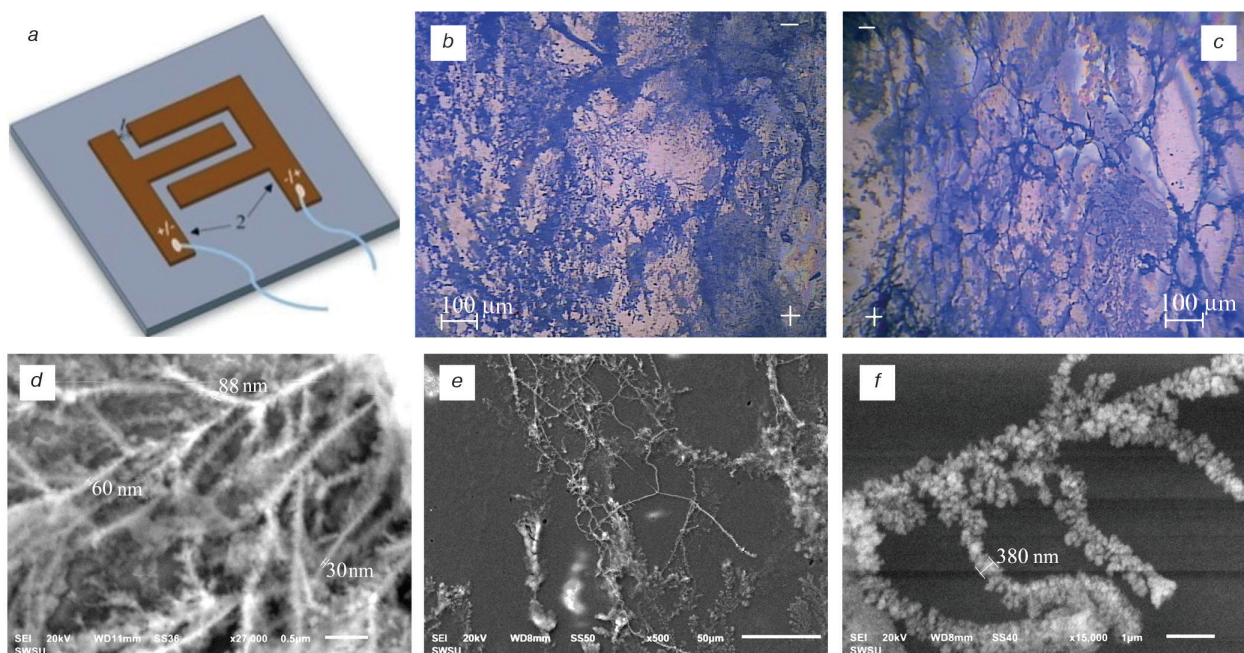


**Figure 2.** (a) IC, (b, c) confocal microscopy and (d–f) SEM images of colloidal solution residue (MWCNT – COOH + aerosil +  $\text{H}_2\text{O}_{\text{dw}}$ ) on sittal; b, c: PLS, FS and DS formation at  $U = 19$  and 19.5 V, respectively; d: FS and PLS formation at  $U = 19$  V; e, f: PLS and DS formation at  $U = 19.5$  V.

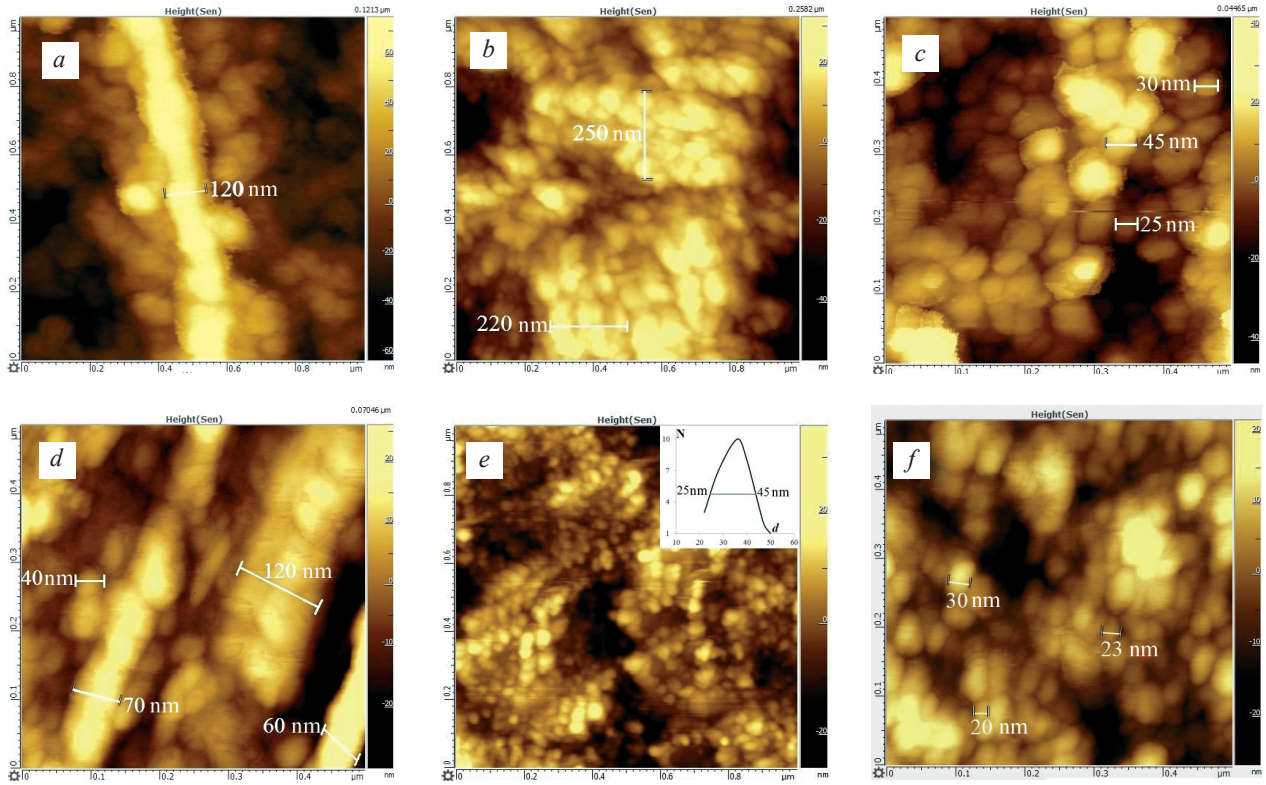


**Figure 3.** AFM images of structures forming from MWCNT – COOH at  $U = 19$  V: *a-c*: PLS, DS and FS from colloidal solution, respectively; *d-f*: at  $U = 19.5$  V PLS, PLS and FS and DS, respectively. Inset: size distribution.

mode”) and  $G = 1567 \div 1600$   $\text{cm}^{-1}$  (tangential oscillations) in the Raman spectra confirmed their MWCNT – COOH affiliation (Fig. 4). The test MWCNT are characterized by a higher number of defects because  $I_D$  and  $I_{2D} > I_G$  and the width of the bands is greater than  $50$   $\text{cm}^{-1}$  [15]. The intensity of the characteristic bands ( $I_D$  and  $I_G$ ) was the highest for the FSs. In the vicinity of DSs this intensity was four times lower and in the vicinity of PLSs the intensity of these bands decreased by an order of magnitude (Fig. 4). By and large the  $I_D/I_G$  ratio which characterizes the defectiveness of MWCNT – COOH + aerosol +  $\text{H}_2\text{O}_{\text{dw}}$  complexes proved to be the lowest for the PLSs (1.17); for the FS and DS it was 1.18 and 1.15, respectively (Table 1). This regularity was also indicated by the  $I_{2D}/I_G$  ratio ( $I_{2D}$  is the two-photon inelastic scattering band) and by the widths of the bands at 0.5 height for  $I_D$ ,  $I_G$  and  $I_{2D}$  which correlate with the residual surface tension in the MWCNT – COOH complexes (Table 1). Their greater defectiveness in comparison with the PLSs significantly reduced the homogeneity region:  $L = 4,4(I_G/I_D)$ . The size of the homogeneity region was as follows:  $\sim 3.76$  nm for the PLSs,  $\sim 3.73$  nm for the FSs and 3.82 nm for the DSs whereas the diameter of the test MWCNT was 20 nm. These homogeneity data ( $L$ ) agreed with coherent scattering region calculations made on the basis of X-ray diffraction patterns (GBC EMMA, 60 kV acceleration voltage, 80 mA current,  $2\theta = 20 \div 120^\circ$  scanning angle range,  $\text{CuK}\alpha$  radiation). Coherent scattering region evaluation with allowance for the Debye-Scherrer condition ( $L = 0,9\lambda/$

**Table 1.** Defect concentration and residual surface stress in biased piecewise linear formations, diffuse structures and fractal structures as per Raman spectroscopy data.

Sample	$I_D/I_G$	$I_{2D}/I_G$	$\Delta I_{D,0.5}$	$\Delta I_{G,0.5}$	$\Delta I_{2D,0.5}$	$L$ , nm
PLS	1.17	0.88	50	51	62	3.76
DS	1.15	0.63	50	51	62	3.82
FS	1.18	0.76	50	62	62	3.73

( $\beta \cos \theta$ )) for MWCNT and MWCNT – COOH yielded 3.12 and 3.5 nm, respectively. Here  $\lambda = 0.1541$  nm is the  $\text{CuK}\alpha$  X-ray radiation wavelength,  $\beta$  is the peak intensity at half height and  $\theta$  is the zero peak position.

The presence of the  $G$  band characterizing violation of symmetrical graphene sheet wrapping showing itself as degeneration of oscillations depending on orientation along ( $G^+ - LO$ ) or across ( $G^- - TO$ ) the nanotube axis is only typical of SWCNT, and this was observed for the DSs and PLSs (Fig. 4). The intensities of these bands met the  $I_G^- > I_G^+$  condition indicating the presence of bends in the MWCNT which was confirmed by AFM data (Fig. 3a).

In the low-frequency spectral region where SWCNT exhibit excitation of radial “breathing” mode at 100 to 600  $\text{cm}^{-1}$ , all the test MWCNT structures (FS, DS and PLS) exhibited untypical excitations (Fig. 4, inset).

Analysis of the experimental AFM images (Fig. 3) showed that the sizes of the structures ( $d$ ) forming the FS, DS and PLS decreased with an increase in voltage (Fig. 5a). Simultaneously the particle velocities ( $V$ ) as indicated by video monitoring increased with DC voltage

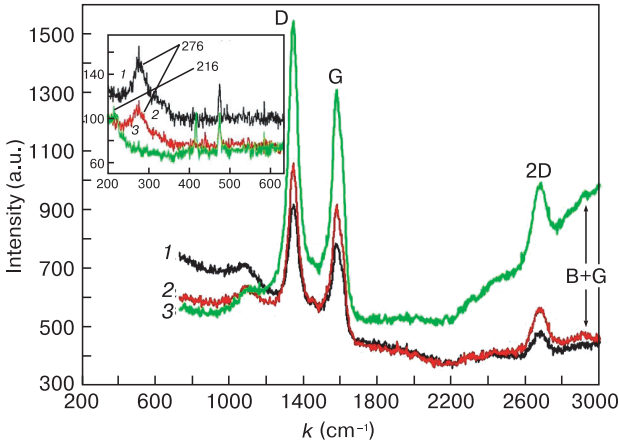


**Figure 4.** Raman spectra of (1) PLS, (2) DS and (3) FS forming from MWCNT – COOH + aerosil + H<sub>2</sub>O<sub>dw</sub>. Inset: radial “breathing” mode region.

amplitude at  $U = 19.5$  V (Fig. 5b). The  $d_s(U)$  and  $V(U)$  dependences were clearly nonlinear. However at each  $U$  the PLS formation rate in the electrode gap changed in a stepwise manner, remaining constant for some time (Fig. 5a). In fact under these conditions the MWCNT – COOH + aerosil + H<sub>2</sub>O<sub>dw</sub> complexes were polarized between the electrodes by the electric field [16]. In accordance with earlier works [11, 17] the dynamic equation  $F_q = qE$  describing the movement of these complexes in a drop of solution enhanced by the electric force acting on polarized colloidal solution complexes with the same charge ( $q_i = q_j = q$ ) takes on as follows in an electric field:

$$m \frac{d\mathbf{v}_i}{dt} = m \left( \frac{\partial \mathbf{V}}{\partial t} + \mathbf{v}(\nabla \mathbf{V}) \right) - \sum_{i \neq j}^N \nabla U(R_{ij}) + \mathbf{F}_s(R_s) + \mathbf{F}_L(R_L) - 6\pi a \eta (\mathbf{v}_i - \mathbf{V}) + \mathbf{F}_B + \mathbf{F}_q. \quad (1)$$

Here  $m[(\partial \mathbf{V}/\partial t) + \mathbf{v}(\nabla \mathbf{V})]$  are the interaction forces allowing for the change in the volume of the drop ( $\mathbf{V}$ );  $U(R_{ij})$  is the particle interaction potential ( $q_i$  and  $q_j$  at the distance  $R_{ij}$ ) in accordance with the Derjaguin–Landau–Verwey–Overbeek theoretical model;  $F_L(R_L)$  and  $F_s(R_s)$  are the interaction forces with the substrate and the liquid/air phase boundary, respectively;  $6\pi R \eta (\mathbf{v}_i - \mathbf{V})$  is the Stokes viscous friction force;  $F_B$  is the random Brownian motion force of Gaussian type.

Comparison between the contributions of all the forces in Eq. (1) complicates the analytical solution of this equation which was only solved numerically [17]. In accordance with the data presented in Fig. 5, the formation of FS, DS and PLS can be analyzed with reducing Eq. (1) to only the most important force  $F_q$ . Along with this force, the interaction between polarized particles in the colloidal solution requires Coulomb’s force  $F_c = q_i q_j / (4\pi \epsilon_1 \epsilon_0 R^2)$  be taken into account. It is Coulomb’s force that leads to the agglomeration (coagulation) of polarized colloidal solu-

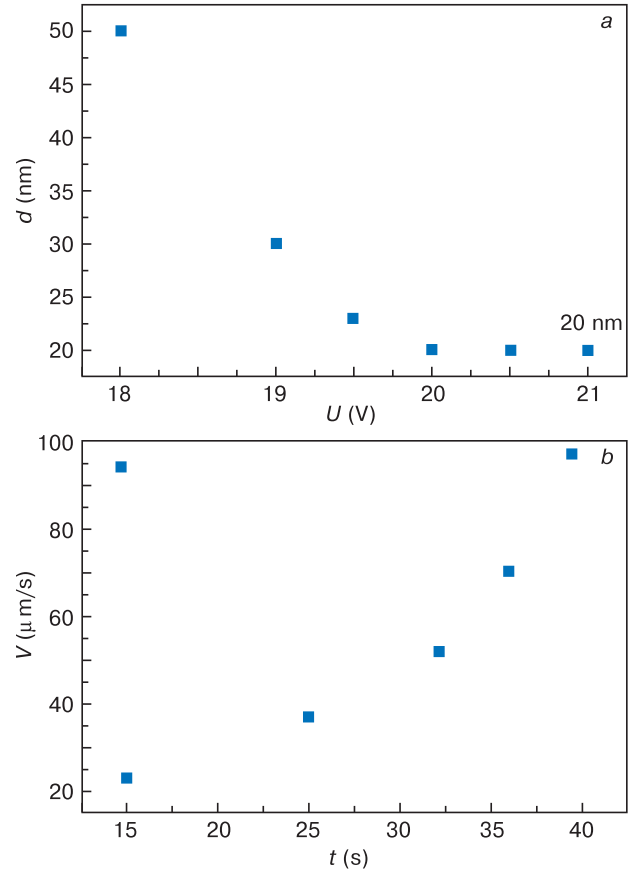


**Figure 5.** (a) size and (b) growth rate of nanostructures as a function of DC voltage amplitude as determined from AFM images and video monitoring at  $U = 19.5$  V, respectively.

tion complexes into stable structures as can be seen from Fig. 3. To describe the formation of these structures in an electric field we will use earlier conclusions [13]. In accordance with [13] these structures are affected in this case by the electrophoretic force:

$$F_{EF} = 2\pi \epsilon_1 \text{Re}[K(\omega)] R^3 \nabla E^2, \quad (2)$$

where  $\epsilon_1$  and  $\epsilon_2$  are the dielectric permeabilities of the medium ( $\epsilon_1 = \epsilon_{\text{H}_2\text{O}} = 81$ ) and the particles, respectively;  $\sigma_1$  and  $\sigma_2$  are the dielectric conductivities of the medium and the particles, respectively;  $\omega$  is the AC field frequency;  $\text{Re}[K(\omega)] = [(\epsilon_2 - \epsilon_1)/(\epsilon_2 + 2\epsilon_1)] + \{3(\epsilon_1 \sigma_2 - \epsilon_2 \sigma_1) / [\tau_{\text{MW}}(\sigma_2 + 2\sigma_1)^2(1 + \omega^2 \tau_{\text{MW}}^2)]\}$  is the real part of the Clausius–Mosotti function;  $E$  is the electric field magnitude;  $R$  is the particle radius;  $\tau_{\text{MW}} = (\epsilon_2 + 2\epsilon_1) / (\sigma_2 + 2\sigma_1)$  is the particle recharging time (Maxwell–Wagner charge relaxation time) in AC electric fields. In DC electric fields ( $\omega = 0$ )  $K(\omega) = 1$  and Eq. (1) simplifies to:

$$F_{EF} = 2\pi \epsilon_1 R^3 \nabla E^2. \quad (3)$$

In order for nanostructures in the form of PLS or FS to be equilibrium, their growth from colloidal solutions in an electric field should probably satisfy the following equation:

$$F_{\text{EF}} = F_q = q^2/(4\pi\epsilon_1\epsilon_0R^2) = qE.$$

In order for  $N$  complexes of a colloidal solution with the radius  $R$  to fill the electrode gap  $Z$  the equality  $Z = 2NR$  should be met. The change in the size of the MWCNT – COOH complexes as a function of applied bias  $d = f(U)$  can be derived from Eq. (3) taking into account that  $E = U/Z$ . The change  $\max(\nabla E^2)$  at  $d \rightarrow 2R$  will obey the hyperbolic law  $d = 1/U$ , in agreement with experimental data (Fig. 5a). The minimum size of the structures (Figs 2, 3) is close to the size of MWCNT:  $d = 2R = 20$  nm (Fig. 1, inset).

Basing on the fact that the particles move mainly due to the electrophoretic force (Eq. (2)), one can convert the motion equation  $F_{\text{EF}} = mdv/dt$  at a constant field magnitude to the following empirical function:

$$V(U) = \frac{3}{2}(\rho)^{-1}\epsilon_1E^2 \int dt = v_0 + BE^2, \quad (4)$$

where  $v_0$  is the initial velocity determined by diffusion and convection of particles in the test colloidal solution;  $\rho$  is the density of carbon particles;  $B$  is the constant that accounts for  $\rho$ ;  $\epsilon_1$  is the dielectric permeability of the liquid phase of the colloidal solution;  $Z$  is the electrode gap which was 100, 500, 1000 or 1500  $\mu\text{m}$  in the experiment;  $t$  is the evaporation time of a solution drop (3.5 min).

A Raman spectrum taken in perpendicular radiation incidence and scattering geometry contained bands in the radial “breathing” mode region that are only typical of SWCNT (in PLS and DS ( $276\text{ cm}^{-1}$ ) and FS ( $216\text{ cm}^{-1}$ ), see Fig. 4 (inset). This indicates the presence of SWCNT inside MWCNT which could only be oriented perpendicular to the substrate. Thus the entire MWCNT structure with SWCNT inside must be arranged vertically relative to the substrate. Earlier SWCNT were identified inside MWCNT by high resolution transmission electron microscopy [18] and Raman spectroscopy [19, 20]. They had very small diameters (0.4 nm), were oriented only along the multiwalled nanotube axes and located on nanotube ends. Theoretically estimated diameters of the SWCNT observed in this experiment made based on the spectral bands from the  $d \sim 285\text{ cm}^{-1}/\omega$  ratio [21] were  $\sim 1$  nm for the PLS and the DS and  $\sim 1.4$  nm for the FS.

## References

1. Lehman J.H., Terrones M., Mansfield E., Hurst K.E., Meunier V. Evaluating the characteristics of multiwall carbon nanotubes. *Carbon*, 2011; 49(8): 2581–2602. <https://doi.org/10.1016/j.carbon.2011.03.028>
2. Prasek J., Drbohlavova J., Chomoucka J., Hubalek J., Jasek O., Adam V., Kizek R. Methods for carbon nanotubes synthesis – review. *J. Mater. Chem.*, 2011; 21: 15872–15884. <https://doi.org/10.1039/c1jm12254a>
3. De Volder M.F.L., Tawfick S.H., Baughman R.H., Hart A.J. Carbon nanotubes: Present and future commercial applications. *Science*, 2013; 339(6119): 535–539. <https://doi.org/10.1126/science.1222453>
4. Sameera I., Bhatia R., Prasad V., Menon R. High emission currents and low threshold fields in multi-wall carbon nanotube-polymer composites in the vertical configuration. *J. Appl. Phys.*, 2012; 111(4): 044307(5). <https://doi.org/10.1063/1.3685754>
5. Yuchi Che, Haitian Chen, Hui Gui, Jia Liu, Bilu Liu and Chongwu Zhou. Review of carbon nanotube nanoelectronics and macroelectronics. *Semicond. Sci. Technol.*, 2014; 29(7): 073001(17). <https://doi.org/10.1088/0268-1242/29/7/073001>

At an excitation energy of 2.33 eV (532 nm), taking into account the Kataura Table [22] and the Raman spectrum data for the radial “breathing” mode region (Fig. 4, inset) the  $276\text{ cm}^{-1}$  band pertains to SWCNT with the chirality (10, 1) and the angle in the range  $0 < \theta < 30^\circ$ . Thus, the PLSs (Fig. 3a, d) and the DSs (Fig. 3b, f) have combined conductivity: 1/3 metallic and 2/3 semiconductor. This is also testified to by the bends in the PLSs (Fig. 3a) corresponding to combined  $sp^2$ -hybridization with  $\pi$ -bound elongated carbon clusters (sized up to several decades of microns in the form of PLSs) or with  $\sigma$ -bound DS structures. The excitation of oscillations in the FSs (Fig. 3c, e, band at  $216\text{ cm}^{-1}$ ) has the chirality (9, 7) following this classification.

## 4. Conclusion

Self-assembly and/or self-organization in purified and functionalized MWCNT – COOH + aerosil +  $\text{H}_2\text{O}_{\text{dw}}$  produces diffuse structures, fractal structures or local piecewise formations the sizes of which obey the  $1/U$  law and the growth rate of which obeys the  $U^2$  law. MWCNT – COOH + aerosil +  $\text{H}_2\text{O}_{\text{dw}}$  complexes are oriented in a controlled manner in electric fields. We show that intense ultrasonication of MWCNT – COOH + aerosil +  $\text{H}_2\text{O}_{\text{dw}}$  complexes produces axis centered SWCNT inside MWCNT as confirmed by Raman scattering excitation in the short wave region (radial “breathing” modes). The variety of structures forming in DC electric fields is caused by the existence of combined  $sp^2$ -hybridization types with  $\pi$ - and  $\sigma$ - carbon bonds and the metallic and semiconductor conductivity types in the material which alone shows good promise of these structures for nanoelectronics.

## Acknowledgements

The work was performed with financial support of the Ministry of Education and Science of the Russian Federation within the basic part of State Assignment No. 16.2814.2017/PCh (Project No. 39.13) and Agreement No. 14.577.21.0181 (unique ID RFMEFI57715X0181).

6. Ageev O.A., Blinov Y.F., Il'ina M.V., Il'in O.I., Smirnov V.A., Tsukanova O.G. Study of adhesion of vertically aligned carbon nanotubes to a substrate by atomic-force microscopy. *Phys. Solid State*, 2016; 58(2): 309–314. <https://doi.org/10.1134/S1063783416020037>
7. Sergeev G.B. Dimensional effects in nanochemistry. *Rossiiskii khimicheskii zhurnal = Russian J. General Chemistry*, 2002; XLVI(5): 22–29. (In Russ.)
8. Vorob'eva A.I. Equipment and techniques for carbon nanotube research. *Phys. Usp.*, 2010; 53(3): 257–277. <https://doi.org/10.3367/UFNe.0180.201003d.0265>
9. Reinert L., Zeiger M., Suárez S., Presser V., Mücklich F. Dispersion analysis of carbon nanotubes, carbon onions, and nanodiamonds for their application as reinforcement phase in nickel metal matrix composites. *RSC Adv.*, 2015; 5(115): 95149–95159. <https://doi.org/10.1039/C5RA14310A>
10. Van Thu Le, Cao Long Ngo, Quoc Trung Le, Trinh Tung Ngo, Duc Nghia Nguyen, Minh Thanh Vu. Surface modification and functionalization of carbon nanotube with some organic compounds. *Adv. Nat. Sci.: Nanosci. Nanotechnol.*, 2013; 4(3): 035017 (5pp). <https://doi.org/10.1088/2043-6262/4/3/035017>
11. Kuz'menko A.P., Aung Ch.N., Rodionov V.V. 3D fractalization over natural colloidal microinclusions. *Tech. Phys.*, 2015; 60(6): 903–910. <https://doi.org/10.1134/S1063784215060146>
12. Kuzmenko A.P., Thet Phyto Naing, Myo Min Than, Dovolamislov M.B., Chan Nyein Aung. Process of self-organization in carbon containing colloidal solution. *Izvestiya Yugo-Zapadnogo gosudarstvennogo universiteta. Seriya tekhnika i tekhnologii = Proceedings of the Southwest State University. Technics and Technologies*, 2015; (3): 38–50. (In Russ.)
13. Kuzmenko A.P., Thet Phyto Naing, Myo Min Than, Chan Nyein Aung, Dobromyslov M. B., Emelyanov S.G., Chervyakov L.M. Self-assembly and self-organization processes of carbon nanotubes in the colloidal systems. *J. Nano- Electron. Phys.*, 2015; 7(4): 04014(3pp).
14. Velev O.D., Bhatt K.H. On-chip micromanipulation and assembly of colloidal particles by electric fields. *Soft Matter.*, 2006; 2(9): 738–750. <https://doi.org/10.1039/b605052b>
15. Krupke R., Hennrich F., von Löhneysen H., Kappes M.M. Separation of metallic from semiconducting single-walled carbon nanotubes. *Science*, 2003; 301(5631): 344–347. <https://doi.org/10.1126/science.1086534>
16. Ma Shao-Jie, Guo Wan-Lin. Mechanism of carbon nanotubes aligning along applied electric field. *Chinese Phys. Lett.*, 2008; 25(1): 270–273. <https://doi.org/10.1088/0256-307X/25/1/073>
17. Andreeva L.V., Koshkin A.V., Lebedev-Stepanov P.V., Petrov A.N., Alfimov M.V. Driving forces of the solute self-organization in an evaporating liquid microdroplet. *Colloids and Surfaces A: Physicochem. Eng. Aspects.*, 2007; 300(3): 300–306. <https://doi.org/10.1016/j.colsurfa.2007.02.001>
18. Lu-Chang Qin, Xinluo Zhao, Kaori Hirahara, Yoshiyuki Miyamoto, Yoshinori Ando, Sumio Iijima. The smallest carbon nanotubes. *Nature*, 2000; 408(6808): 50. <https://doi.org/10.1038/35040699>
19. Dresselhaus M.S., Jorio A., Hofmann M., Dresselhaus G., Saito R. Perspectives on carbon nanotubes and graphene Raman spectroscopy. *Nano Lett.*, 2010; 10(3): 751–758. <https://doi.org/10.1021/nl904286r>
20. Zhao X., Ando Y., Qin L.-C., Kataura H., Maniwa Y., Saito R. Characteristic Raman spectra of multiwalled carbon nanotubes. *Physica B: Condensed Matter*, 2002; 323(1): 265–266. [https://doi.org/10.1016/S0921-4526\(02\)00986-9](https://doi.org/10.1016/S0921-4526(02)00986-9)
21. Thomsen C., Reich S. Raman Scattering in Carbon Nanotubes. In: *Light Scattering in Solid IX. Topics in Applied Physics*. Vol. 108. Berlin; Heidelberg: Springer, 2006: 115–234. [https://doi.org/10.1007/978-3-540-34436-0\\_3](https://doi.org/10.1007/978-3-540-34436-0_3)
22. Maultzsch J., Telg H., Reich S., Thomsen C. Radial breathing mode of single-walled carbon nanotubes: Optical transition energies and chiral-index assignment. *Phys. Rev. B.*, 2005; 72(20): 205438(1–16). <https://doi.org/10.1103/PhysRevB.72.205438>